An All-Purpose Transmission-Line Model for Interconnect Simulation in SPICE

Mustafa Celik, *Member, IEEE,* Andreas C. Cangellaris, *Member, IEEE,* and Abdul Yaghmour

***Abstract*— A new all-purpose multiconductor transmission-line model is described for efficient and robust interconnect simulation using nonlinear circuit simulators such as SPICE. All types of interconnects, i.e., uniform, nonuniform, lossless, lossy/dispersive, can be handled by the proposed model. Furthermore, coupling of electromagnetic radiation to interconnects can be directly modeled without the need for developing a new subcircuit. Another advantage of the proposed model is that it enables sensitivity analysis with respect to both circuit and interconnect parameters, thus facilitating interconnect circuit optimization. Chebyshev expansions for the spatial variations of the interconnect voltages and currents are used to effect highly accurate numerical approximations of the Telegrapher's equations using as small a number of degrees of freedom as possible. A simple rule of thumb is provided for the selection of the order of the approximation given the frequency bandwidth of interest. Numerical examples are presented to demonstrate the validity of the proposed model and illustrate its application to a variety of interconnect-induced noise interactions in high-speed electronic systems.**

***Index Terms*— Circuit transient analysis, distributed parameter circuits, integrated circuit interconnections, multiconductor transmission lines, packaging, simulation.**

I. Introduction

THE RAPID growth in size, density, and complexity of modern integrated circuits, combined with the quest for several hundred megahertz clock frequencies, has made the use of transmission-line modeling of interconnects a requirement for all state-of-the-art circuit simulators. Such transmission-line modeling capability allows distributed electromagnetic effects, such as long interconnect-induced delays and crosstalk, as well as package-induced inductive noise, to be taken into account for accurate electrical performance prediction and proper power/signal distribution network design.

Over the past 15 years a variety of models have been proposed for interconnect simulation. In most cases, their development was driven by the desire to effect computationally efficient and accurate interconnect simulation within the framework of nonlinear circuit simulators such as SPICE [1]–[11]. Such models are extremely important to electrical performance evaluation of integrated electronic systems, since they facilitate the simulation of these systems within a familiar and well-established circuit simulation environment.

A comparison of the aforementioned transmission-line models reveals variability in their modeling accuracy and computation efficiency, which is due to one or more of the following factors:

1) physical properties of interconnects;
2) bandwidth of interest to specific transient simulation;
3) specific design application.

For example, the method of characteristics is ideal for modeling lossless transmission lines; however, its extension to lossy dispersive interconnects becomes computationally inefficient, especially for lines which are electrically long and exhibit significant loss. (For the purposes of this discussion, a transmission line is considered to be *electrically long* when its length spans several wavelengths at the upper frequencies in the bandwidth of interest). While one might argue that for such types of interconnects model order-reduction techniques such as the asymptotic waveform evaluation (AWE) and its enhancements provide a computationally efficient alternative [5], [9], [11], the stability of the circuit resulting from the connection of the generated macromodels with other nonlinear driving and receiving electronics still remains an issue of concern.

From the above discussion, it becomes obvious that a single all-purpose transmission-line model that can provide highly accurate broad-band performance without penalizing efficiency is not available yet. Instead, *hybrid* approaches are being proposed where, with the frequency range of validity and computation efficiency of several models properly quantified, a selection of the *optimal model* is made based on a predetermined modeling error and desired computation efficiency [12].

Even though such a *hybrid* approach is very sensible from an engineering point of view, there are important advantages associated with the availability of the single all-purpose transmission-line model mentioned above. First and foremost, such an all-purpose model equipped with an *a priori* estimate of its accuracy becomes an invaluable tool for evaluation and verification of other models, especially for those cases that the aforementioned *hybrid* approach is used. Second, there is a definitive simplicity associated with the use of a single general model that is hard to overlook. In essence, a transmission-line system becomes simply another "element" in the circuit simulator, handled the same way no matter what its per-

Manuscript received January 28, 1997; revised May 16, 1997. This work was supported in part by the Semiconductor Research Corporation under Contract 95-PP-086.

M. Celik is with the Department of Electrical and Computer Engineering, Carnegie–Mellon University, Pittsburgh, PA 15213 USA.

A. C. Cangellaris was with the Department of Electrical and Computer Engineering, University of Arizona, Tucson, AZ 85721 USA. He is now with the Department of Electrical and Computer Engineering, University of Illinois at Urbana–Champaign, Urbana, IL 61801 USA.

A. Yaghmour is with the Center for Electronic Packaging Research, Department of Electrical and Computer Engineering, University of Arizona, Tucson, AZ 85721 USA.

Publisher Item Identifier S 0018-9480(97)07400-0.

unit-length electrical properties might be. In addition, if the model can support sensitivity analysis with respect to both circuit and interconnect parameters, it becomes an invaluable tool for efficient interconnect optimization. Finally, the use of such a model for accurate simulation during the final stages of design (for the purpose of design verification) is highly desirable, especially if the model is compatible with model-order reduction schemes.

The description of such an all-purpose transmission-line model is the subject of this paper. This model was originally presented in [13] as part of a methodology for the application of Krylov subspace order-reduction techniques for linear circuits containing transmission lines. In Section II, the fundamental steps in the development of the model are reviewed. Section III deals with issue of the proper selection of the order of the numerical approximation and establishes relevant selection rules. In Section IV, the incorporation of the proposed transmission-line model into the modified nodal-admittance (MNA) matrix equations is presented, and the application of the resulting circuit model for sensitivity analysis is discussed. Section V presents model validation studies as well as several examples from the application of the proposed model to the analysis of transmission-line circuits. Finally, some concluding remarks are given in Section VI.

II. Development of the New Transmission-Line Model

In addition to modeling crosstalk and interconnect delay effects, transmission-line theory can be successfully used for the modeling of the coupling of electromagnetic radiation to interconnects. By now, the physics of this electromagnetic interaction is well understood [14]. More specifically, it is generally accepted that if the quantities of interest are the induced voltages and currents at the interconnect terminations, transmission-line theory leads to results of sufficient engineering accuracy. In particular, under the assumption that the cross-sectional dimensions of the multiconductor transmission line (MTL) are small compared to the minimum wavelength of interest in the incident electromagnetic fields, the distribution of voltages and currents along the N conductors of an $N+1$ conductor MTL with the $(N+1)$st conductor taken as reference is described by a hyperbolic system which has the following form in the Laplace domain:

$$\frac{d}{dx'}\boldsymbol{V}(x',s) = -(\boldsymbol{R}(x') + s\boldsymbol{L}(x'))\boldsymbol{I}(x',s) + \boldsymbol{P}(x',s) \quad (1)$$

$$\frac{d}{dx'}\boldsymbol{I}(x',s) = -(\boldsymbol{G}(x') + s\boldsymbol{C}(x'))\boldsymbol{V}(x',s) + \boldsymbol{W}(x',s) \quad (2)$$

where, $\boldsymbol{V}(x',s)$ and $\boldsymbol{I}(x',s)$ are, respectively, the column vectors of the N line voltages and currents, $\boldsymbol{R}(x')$, $\boldsymbol{L}(x')$, $\boldsymbol{C}(x')$, and $\boldsymbol{G}(x')$ are, respectively, frequency independent per-unit-length resistance, inductance, capacitance, and conductance $N \times N$ matrices, and s is the Laplace variable. The more general case of transmission lines with frequency-dependent per-unit-length matrices is discussed in detail in [13]. $\boldsymbol{P}(x',s)$ and $\boldsymbol{W}(x',s)$ are column vectors of length N that incorporate the effect of the incident radiation in the form of distributed sources. These voltage and current sources are dependent on the physical properties of the interconnects and can be computed using the results in [15], [16].

The general approach to include the MTL systems into a circuit simulator is to treat them as linear multiports described by a suitable relationship between terminal voltages and currents

$$\boldsymbol{A}(s)\boldsymbol{V}_t(s) + \boldsymbol{B}(s)\boldsymbol{I}_t(s) = \boldsymbol{F}(s) \quad (3)$$

where $\boldsymbol{V}_t(s)$ and $\boldsymbol{I}_t(s)$ are column vectors containing, respectively, the terminal voltages and currents of the multiconductor-line system, while $\boldsymbol{F}(s)$ describes the effect of all sources present along the transmission line. The matrices $\boldsymbol{A}(s)$ and $\boldsymbol{B}(s)$ are described in terms of the per-unit-length MTL parameters. In order for the above equations to be compatible with the MNA formalism, these matrices must be first-degree polynomials in s.

To achieve this, the linearity in s of the left-hand side (LHS) of (1) and (2) suggests an approximation in which spatial derivatives are calculated explicitly and terminal voltages and currents appear explicitly in the resulting approximation. The most direct way to effect such an approximation is to segment the transmission line into sections of length Δl, which is chosen to be a small fraction of the wavelength, and using a lumped-element circuit model for each section with series elements $L(\Delta l)$, $R(\Delta l)$, and shunt elements $G(\Delta l)$, $C(\Delta l)$. The disadvantage of such an approach is that the choice of Δl depends not only on the minimum wavelength of interest in the simulation, but also on the electrical length (i.e., the length in wavelengths) of the interconnect. More specifically, theoretical and numerical studies have shown that the number of segments per wavelength needs to increase as the electrical length of the interconnect increases, in order to keep the numerical dispersion error and, hence, the artificial distortion of the propagating pulses below a desirable level [17], [18]. As an example, consider a 10-cm interconnect embedded in a dielectric with relative dielectric constant of nine. If the maximum frequency of interest in the simulation is 10 GHz, the corresponding minimum wavelength is easily found to be 1 cm. Hence, the line has an electrical length of ten, and the results in [18] suggest that the number of segments per wavelength should be 26, resulting in a total of 260 segments for the approximation of the transmission line. Clearly, such a large number of segments is unacceptable, since it results in very large numbers of lumped-circuit elements, especially when dealing with MTL's.

The alternative to the aforementioned segmentation is the use of spectral expansions for the representation of the voltage and current distributions along the interconnects. Spectral approximations exhibit exponential convergence, and thus, highly accurate numerical solutions can be achieved with as few as three degrees of freedom per wavelength [19]. The implementation of such spectral approximations for the transient analysis of high-speed interconnects was originally proposed by Palusinski and Lee [20], and later used by others for the analysis of nonuniform transmission lines [21], [22]. In that work, a rigorous Galerkin procedure was used in conjunction with Chebyshev polynomial expansions for the representation of the spatial variation of the interconnect voltages and currents. Chebyshev expansions were also used

for the representation of the position-dependent per-unit-length transmission-line parameters. However, use of the Galerkin's process results in a rather complicated discrete model, making its direct incorporation in standard-circuit simulators rather cumbersome. This is especially true when dispersive interconnects with frequency-dependent losses need be modeled.

The model proposed in this paper is based on an alternative discretization approach, commonly referred to as *pseudo-spectral* approximation. As will become apparent from the technical discussion that follows, this approach leads to a much simpler discrete model that can be interfaced with existing SPICE-like circuit simulators in a very simple and direct fashion.

A. Two-Conductor Transmission Line

The development begins with the simple case of a two-conductor transmission line of length l, i.e., $(0 \leq x' \leq l)$. The transformation $x = 2x'/l - 1$ is used to map the domain $[0, l]$ onto the domain $[-1, 1]$. Let $V(x_n, s), I(x_n, s), P(x_n, s), W(x_n, s), n = 0, 1, 2, \cdots, M$ be the values of voltage, current, and distributed sources at the points x_n defined by

$$x_n = \cos\frac{\pi n}{M}, \qquad n = 0, 1, \cdots, M. \tag{4}$$

Clearly, $x_0 = 1$ and $x_M = -1$ correspond, respectively, to the far- and near-end terminals of the transmission line. It can be shown that the use of the Chebyshev polynomials of type 1 $T_m(x) = \cos(m \cos^{-1} x)$ for the approximation of the spatial variation of the line voltage, current, and distributed sources lead to the following expressions [13]:

$$V(x, s) = \sum_{m=0}^{M} V(x_m, s) g_m(x) \tag{5}$$

$$I(x, s) = \sum_{m=0}^{M} I(x_m, s) g_m(x) \tag{6}$$

$$P(x, s) = \sum_{m=0}^{M} P(x_m, s) g_m(x) \tag{7}$$

$$W(x, s) = \sum_{m=0}^{M} W(x_m, s) g_m(x) \tag{8}$$

where M is the number of polynomials used in the expansions, $g_m(x)$ are given by

$$g_m(x) = \frac{(1 - x^2) T'_M(x) (-1)^{m+1}}{c_m M^2 (x - x_m)} \tag{9}$$

and c_m is defined as

$$c_m = \begin{cases} 2, & m = 0, M \\ 1, & \text{otherwise.} \end{cases} \tag{10}$$

It is noted that the polynomials $g_m(x)$ have the Lagrange polynomial-type property

$$g_m(x_n) = \delta_{mn} \tag{11}$$

where δ_{mn} is the Kronecker delta.

In order to construct the numerical approximation of Telegrapher's equations, a collocation method is used with collocation points such as those in (4). Substitution of (5) and (6) into Telegrapher's equations, and use of the fact that the derivatives of the polynomials g_m at the collocation points are known in closed form [19], leads to the following system of linear equations:

$$\sum_{m=0}^{M} V(x_m, s) D_{nm} = -\frac{l}{2}[R(x_n) + sL(x_n)] I(x_n, s) + \frac{l}{2} P(x_n, s) \tag{12}$$

$$\sum_{m=0}^{M} I(x_m, s) D_{nm} = -\frac{l}{2}[G(x_n) + sC(x_n)] V(x_n, s) + \frac{l}{2} W(x_n, s) \tag{13}$$

for $n = 0, 1, \cdots, M$, where

$$\left.\frac{d}{dx} g_m(x)\right|_{x = x_n} = D_{nm}. \tag{14}$$

Let $\boldsymbol{D}$ be the $(M+1) \times (M+1)$ square matrix with elements D_{nm}. Then, the above system of equations may be cast in matrix form as follows:

$$\boldsymbol{D}\boldsymbol{V}_s(s) = -\boldsymbol{Z}(s)\boldsymbol{I}_s(s) + \boldsymbol{P}_s(s) \tag{15}$$

$$\boldsymbol{D}\boldsymbol{I}_s(s) = -\boldsymbol{Y}(s)\boldsymbol{V}_s(s) + \boldsymbol{W}_s(s) \tag{16}$$

where

$$\boldsymbol{V}_s(s) = [V(x_0, s), \cdots, V(x_M, s)]^T$$
$$\boldsymbol{I}_s(s) = [I(x_0, s), \cdots, I(x_M, s)]^T$$
$$\boldsymbol{P}_s(s) = \frac{l}{2}[P(x_0, s), \cdots, P(x_M, s)]^T$$
$$\boldsymbol{W}_s(s) = \frac{l}{2}[W(x_0, s), \cdots, W(x_M, s)]^T$$

and, $\boldsymbol{Z}(s)$ and $\boldsymbol{Y}(s)$ are diagonal matrices

$$\boldsymbol{Z}(s) = \frac{l}{2}\,\mathrm{diag}\{R(x_0) + sL(x_0), R(x_1) + sL(x_1), \cdots, R(x_M) + sL(x_M)\} \tag{17}$$

$$\boldsymbol{Y}(s) = \frac{l}{2}\,\mathrm{diag}\{G(x_0) + sC(x_0), G(x_1) + sC(x_1), \cdots, G(x_M) + sC(x_M)\}. \tag{18}$$

The next step in the development of the model deals with the restructuring of (15) and (16) in the desirable form of (3). For this purpose, we use the following colon notation to select specific rows and columns of a matrix. Let $\boldsymbol{A}$ be a matrix. Then $\boldsymbol{A}_{(i:j,m:n)}$ is the $(j-i+1) \times (m-n+1)$ submatrix of $\boldsymbol{A}$ which is between the ith and jth rows, and mth and nth columns of $\boldsymbol{A}$. Similarly, $\boldsymbol{A}_{(i:j,m)}$ is a column vector of length $(j-i+1)$ having as elements the elements of the mth column of the matrix $\boldsymbol{A}$ between (and including) rows i and j. Recognizing that (12) and (13) constitute the approximation of a two-point boundary-value problem, two boundary conditions (involving the values of terminal voltages or the values of the terminal currents or impedance relationships between the terminal

voltages and currents) need to be specified for the problem to be well posed. This implies that two of the equations in (12) and (13) associated with the terminal quantities need to be eliminated in favor of the aforementioned boundary conditions. Without loss of generality, the first and last of the equations in (12) are the ones eliminated. Consequently, using the aforementioned colon notation, (15) and (16) are cast in the following form:

$$\begin{bmatrix} \boldsymbol{D}_a & \boldsymbol{D}_b \\ \boldsymbol{Y}_a(s) & \boldsymbol{Y}_b(s) \end{bmatrix} \begin{bmatrix} V_{\text{near}}(s) \\ V_{\text{far}}(s) \end{bmatrix} + \begin{bmatrix} \boldsymbol{Z}_a(s) & -\boldsymbol{Z}_b(s) & \boldsymbol{Z}_c(s) & \boldsymbol{D}_c \\ \boldsymbol{D}_d & -\boldsymbol{D}_e & \boldsymbol{D}_f & \boldsymbol{Y}_c(s) \end{bmatrix} \begin{bmatrix} I_{\text{near}}(s) \\ I_{\text{far}}(s) \\ \hat{\boldsymbol{I}}_s(s) \\ \hat{\boldsymbol{V}}_s(s) \end{bmatrix} = \begin{bmatrix} \boldsymbol{P}_s(s) \\ \boldsymbol{W}_s(s) \end{bmatrix} \tag{19}$$

where the following array notation has been used:

$$\begin{aligned} \boldsymbol{D}_a &= \boldsymbol{D}_{(2:M,M+1)} \\ \boldsymbol{D}_b &= \boldsymbol{D}_{(2:M,1)} \\ \boldsymbol{D}_c &= \boldsymbol{D}_{(2:M,2:M)} \\ \boldsymbol{D}_d &= \boldsymbol{D}_{(1:M+1,M+1)} \\ \boldsymbol{D}_e &= \boldsymbol{D}_{(1:M+1,1)} \\ \boldsymbol{D}_f &= \boldsymbol{D}_{(1:M+1,2:M)} \\ \boldsymbol{Y}_a(s) &= \boldsymbol{Y}_{(1:M+1,M+1)}(s) \\ \boldsymbol{Y}_b(s) &= \boldsymbol{Y}_{(1:M+1,1)}(s) \\ \boldsymbol{Y}_c(s) &= \boldsymbol{Y}_{(1:M+1,2:M)}(s) \\ \boldsymbol{Z}_a(s) &= \boldsymbol{Z}_{(2:M,M+1)}(s) \\ \boldsymbol{Z}_b(s) &= \boldsymbol{Z}_{(2:M,1)}(s) \\ \boldsymbol{Z}_c(s) &= \boldsymbol{Z}_{(2:M,2:M)}(s). \end{aligned}$$

Also, $V_{\text{near}}(s) = V(x_M, s), V_{\text{far}}(s) = V(x_0, s), I_{\text{near}}(s) = I(x_M, s), I_{\text{far}}(s) = -I(x_0, s)$, while

$$\hat{\boldsymbol{V}}_s(s) = [V(x_1, s) \cdots V(x_{M-1}, s)]^T \tag{20}$$

$$\hat{\boldsymbol{I}}_s(s) = [I(x_1, s) \cdots I(x_{M-1}, s)]^T. \tag{21}$$

Equation (19) can be written in a compact form as

$$(\boldsymbol{A}^R + s\boldsymbol{A}^I) \begin{bmatrix} V_{\text{near}}(s) \\ V_{\text{far}}(s) \end{bmatrix} + (\boldsymbol{B}^R + s\boldsymbol{B}^I) \begin{bmatrix} I_{\text{near}}(s) \\ I_{\text{far}}(s) \\ \hat{\boldsymbol{I}}_s(s) \\ \hat{\boldsymbol{V}}_s(s) \end{bmatrix} = \begin{bmatrix} \boldsymbol{P}_s(s) \\ \boldsymbol{W}_s(s) \end{bmatrix}. \tag{22}$$

In the time domain, the above equation becomes

$$\boldsymbol{A}^R \begin{bmatrix} v_{\text{near}}(t) \\ v_{\text{far}}(t) \end{bmatrix} + \boldsymbol{A}^I \frac{d}{dt} \begin{bmatrix} v_{\text{near}}(t) \\ v_{\text{far}}(t) \end{bmatrix} + \boldsymbol{B}^R \begin{bmatrix} i_{\text{near}}(t) \\ i_{\text{far}}(t) \\ \hat{\boldsymbol{i}}_s(t) \\ \hat{\boldsymbol{v}}_s(t) \end{bmatrix} + \boldsymbol{B}^I \frac{d}{dt} \begin{bmatrix} i_{\text{near}}(t) \\ i_{\text{far}}(t) \\ \hat{\boldsymbol{i}}_s(t) \\ \hat{\boldsymbol{v}}_s(t) \end{bmatrix} = \begin{bmatrix} \boldsymbol{p}_s(t) \\ \boldsymbol{w}_s(t) \end{bmatrix} \tag{23}$$

which is compatible with the numerical integration algorithm used in SPICE.

B. MTL's

The procedure for MTL's is analogous to the one for a two-conductor line. In this case, the voltage, current, and distributed sources for each conductor are expanded in Chebyshev series. Following the procedure used in the two-conductor line case, the discrete form of Telegrapher's equations for an MTL with N active conductors becomes

$$\begin{bmatrix} \boldsymbol{D} & \cdots & \boldsymbol{0} \\ \vdots & \ddots & \vdots \\ \boldsymbol{0} & \cdots & \boldsymbol{D} \end{bmatrix} \begin{bmatrix} \boldsymbol{V}^1(s) \\ \vdots \\ \boldsymbol{V}^N(s) \end{bmatrix} = -\begin{bmatrix} \boldsymbol{Z}^{11}(s) & \cdots & \boldsymbol{Z}^{1N}(s) \\ \vdots & \ddots & \vdots \\ \boldsymbol{Z}^{N1}(s) & \cdots & \boldsymbol{Z}^{NN}(s) \end{bmatrix} \begin{bmatrix} \boldsymbol{I}^1(s) \\ \vdots \\ \boldsymbol{I}^N(s) \end{bmatrix} + \begin{bmatrix} \boldsymbol{P}^1_{\boldsymbol{S}}(s) \\ \vdots \\ \boldsymbol{P}^N_{\boldsymbol{S}}(s) \end{bmatrix} \tag{24}$$

$$\begin{bmatrix} \boldsymbol{D} & \cdots & \boldsymbol{0} \\ \vdots & \ddots & \vdots \\ \boldsymbol{0} & \cdots & \boldsymbol{D} \end{bmatrix} \begin{bmatrix} \boldsymbol{I}^1(s) \\ \vdots \\ \boldsymbol{I}^N(s) \end{bmatrix} = -\begin{bmatrix} \boldsymbol{Y}^{11}(s) & \cdots & \boldsymbol{Y}^{1N}(s) \\ \vdots & \ddots & \vdots \\ \boldsymbol{Y}^{N1}(s) & \cdots & \boldsymbol{Y}^{NN}(s) \end{bmatrix} \begin{bmatrix} \boldsymbol{V}^1(s) \\ \vdots \\ \boldsymbol{V}^N(s) \end{bmatrix} + \begin{bmatrix} \boldsymbol{W}^1_{\boldsymbol{S}}(s) \\ \vdots \\ \boldsymbol{W}^N_{\boldsymbol{S}}(s) \end{bmatrix} \tag{25}$$

where $\boldsymbol{V}^i(s)$ is the vector of voltage samples along the ith conductor

$$\boldsymbol{V}^i(s) = [V^i(x_0, s) \cdots V^i(x_M, s)]^T$$

$$\boldsymbol{Z}^{ij}(s) = \frac{l}{2} \operatorname{diag}\{R^{ij}(x_0) + sL^{ij}(x_0), \cdots, R^{ij} + sL^{ij}(x_M)\}$$

and $\boldsymbol{P}^i_{\boldsymbol{S}}(s)$ is the vector of the samples of the distributed voltage source along the ith conductor

$$\boldsymbol{P}^i_{\boldsymbol{S}}(s) = \frac{l}{2}[P^i(x_0, s), \cdots, P^i(x_M, s)]^T$$

where $\boldsymbol{I}^i(s), \boldsymbol{Y}^{ij}(s)$, and $\boldsymbol{W}^i_{\boldsymbol{S}}(s)$ are similarly defined. Introducing the vectors of terminal voltages and currents as

$$\boldsymbol{V}_{\text{near}}(s) = [V^1(x_M, s), \cdots, V^N(x_M, s)]^T \tag{26}$$

$$\boldsymbol{V}_{\text{far}}(s) = [V^1(x_0, s), \cdots, V^N(x_0, s)]^T \tag{27}$$

$$\boldsymbol{I}_{\text{near}}(s) = [I^1(x_M, s), \cdots, I^N(x_M, s)]^T \tag{28}$$

$$\boldsymbol{I}_{\text{far}}(s) = -[I^1(x_0, s), \cdots, I^N(x_0, s)]^T \tag{29}$$

and arranging (24) and (25), we obtain (30) shown at the bottom of the following page, where the following notation has been used. The matrix $\hat{\boldsymbol{D}}_{(i:j,m:n)}$ is the N-block diagonal matrix with each block being the matrix $\boldsymbol{D}_{(i:j,m:n)}$. The matrix $\hat{\boldsymbol{Z}}_{(i:j,m:n)}(s)$ is defined as

$$\hat{\boldsymbol{Z}}_{(i:j,m:n)}(s) = \begin{bmatrix} \boldsymbol{Z}^{11}_{(i:j,m:n)}(s) & \cdots & \boldsymbol{Z}^{1N}_{(i:j,m:n)}(s) \\ \vdots & \ddots & \vdots \\ \boldsymbol{Z}^{N1}_{(i:j,m:n)}(s) & \cdots & \boldsymbol{Z}^{NN}_{(i:j,m:n)}(s) \end{bmatrix}. \tag{31}$$

$\hat{\boldsymbol{V}}(s) = [\hat{\boldsymbol{V}}^1(s), \cdots, \hat{\boldsymbol{V}}^N(s)]$ where $\hat{\boldsymbol{V}}^i(s)$ is given in (20). $\hat{\boldsymbol{Y}}_{(i:j,m:n)}(s)$ and $\hat{\boldsymbol{I}}(s)$ are defined similarly to $\hat{\boldsymbol{Z}}_{(i:j,m:n)}(s)$ and $\hat{\boldsymbol{V}}(s)$, respectively. Finally, $\hat{\boldsymbol{P}}_{\boldsymbol{S}}(\boldsymbol{s})$ and $\hat{\boldsymbol{W}}_{\boldsymbol{S}}(\boldsymbol{s})$ are properly rearranged versions of the source vectors in (24) and (25), respectively.

Equation (30) can be simply written as

$$(\boldsymbol{A}^R + s\boldsymbol{A}^I)\boldsymbol{V}_t(s) + (\boldsymbol{B}^R + s\boldsymbol{B}^I)\boldsymbol{J}(s) = \boldsymbol{F}(s) \tag{32}$$

where

$$\boldsymbol{J}(s) = \begin{bmatrix} \boldsymbol{I}_t(s) \\ \hat{\boldsymbol{V}}(s) \\ \hat{\boldsymbol{I}}(s) \end{bmatrix} \tag{33}$$

and $\boldsymbol{V}_t = [\boldsymbol{V}_{\text{near}}^T \; \boldsymbol{V}_{\text{far}}^T]^T, \boldsymbol{I}_t = [\boldsymbol{I}_{\text{near}}^T \; \boldsymbol{I}_{\text{far}}]^T$ are, respectively, the vectors of terminal voltages and currents of the MTL. $\boldsymbol{F}(s)$ represents the distributed sources along the conductors in the MTL.

III. Chebyshev-Approximation Order Selection

Because of the direct compatibility of the MTL model as expressed by (32) with the MNA formalism, its incorporation into a SPICE-like circuit simulator is effected simply by entering (32) as a stamp into the overall circuit matrix. In view of this, the order M of the Chebyshev approximation has a direct impact on the size of the overall circuit matrix.

It was shown in [13] that highly accurate expansions can be effected using as few as four Chebyshev polynomials per wavelength. Thus, for a transmission line of length l, with $\lambda_{\min}$ the minimum wavelength of interest, the order of approximation M is chosen as

$$M = 4\frac{l}{\lambda_{\min}} + 2. \tag{34}$$

For transient simulations, the minimum wavelength is decided on the basis of the maximum frequency $f_{\max}$, which is required for accurate resolution of the rise and fall times of the input waveform. Let $\tau_{\min}$ be the smallest of these two signal parameters. A conservative estimate of $f_{\max}$ is then [12]

$$f_{\max} = \frac{1}{\tau_{\min}}. \tag{35}$$

The criterion in (34) for the selection of M works well for moderately long lines (i.e., lines of length less than $4\lambda_{\min}$). However, for longer lines, a modified Chebyshev pseudospectral method, which leads to a more favorable criterion for the selection of M is recommended. The mathematical attributes of this modified Chebyshev method are discussed in detail in [23]. For the purposes of this paper, we restrict ourselves to an intuitive justification of the method, and discuss its impact on the selection of the order of the expansion and the accuracy of the solution.

It is clear from (4) that the interpolation/collocation points are not uniformly distributed along the line. Furthermore, it is easily confirmed that as the order of Chebyshev expansion increases, the collocation points tend to concentrate at the two end points of the line. This, when combined with the collocation procedure used by the pseudospectral approximation, results in an unnecessary oversampling of the voltages and currents at the end points and an undersampling at the center portions of the line. In addition to loss of accuracy at the higher end of the spectrum, the crowding of the points at the boundaries could also reduce the time step of the numerical integration to much smaller values than what is dictated by the physics of the problem.

A way to overcome these difficulties is by mapping the collocation points of (4) to another set of points such that the minimal spacing near the end points is stretched. A systematic way to effect this stretching was proposed in [23]. It is effected through the following equation for the selection of the collocation points:

$$x_n = \frac{\arcsin(\alpha y_n)}{\arcsin(\alpha)}, \qquad n = 0, 1, \cdots M, \quad 0 \le \alpha \le 1 \tag{36}$$

where

$$y_n = \cos(n\pi/M). \tag{37}$$

This stretching implies that the spatial derivative matrix should be modified. The new derivative matrix $\boldsymbol{D}'$ is given by

$$\boldsymbol{D}' = \boldsymbol{A}\boldsymbol{D} \tag{38}$$

where $\boldsymbol{D}$ is the original derivative matrix and $\boldsymbol{A}$ is a diagonal matrix

$$A_{nn} = \frac{\arcsin(\alpha)\sqrt{1-(\alpha y_n)^2}}{\alpha}. \tag{39}$$

The parameter α determines the amount of stretching. The choice $\alpha = 0$ results in the original collocation points given in (4). Through a series of numerical experiments it was found that best results are obtained when α is chosen to be $\sim$0.9.

As discussed in [23], when the modified Chebyshev method is used, a resolution of two points per wavelength is sufficient for high numerical accuracy. This implies that the order of approximation suggested by (34) can be relaxed. More specifically, when electrically long interconnects need be modeled ($l \ge 4\lambda_{\min}$), the modified Chebyshev pseudospectral expansion is applied with the order of approximation M selected according to the following modified criterion:

$$M = 2.5\frac{l}{\lambda_{\min}} + 2. \tag{40}$$

$$\begin{bmatrix} \hat{\boldsymbol{D}}_{(2:M,M+1)} & \hat{\boldsymbol{D}}_{(2:M,1)} \\ \hat{\boldsymbol{Y}}_{(1:M+1,M+1)}(s) & \hat{\boldsymbol{Y}}_{(1:M+1,1)}(s) \end{bmatrix} \begin{bmatrix} \boldsymbol{V}_{\text{near}}(s) \\ \boldsymbol{V}_{\text{far}}(s) \end{bmatrix}$$
$$+ \begin{bmatrix} \hat{\boldsymbol{Z}}_{(2:M,M+1)}(s) & -\hat{\boldsymbol{Z}}_{(2:M,1)}(s) & \hat{\boldsymbol{Z}}_{(2:M,2:M)}(s) & \hat{\boldsymbol{D}}_{(2:M,2:M)} \\ \hat{\boldsymbol{D}}_{(1:M+1,M+1)} & -\hat{\boldsymbol{D}}_{(1:M+1,1)} & \hat{\boldsymbol{D}}_{(1:M+1,2:M)} & \hat{\boldsymbol{Y}}_{(1:M+1,2:M)}(s) \end{bmatrix} \begin{bmatrix} \boldsymbol{I}_{\text{near}}(s) \\ \boldsymbol{I}_{\text{far}}(s) \\ \hat{\boldsymbol{I}}(s) \\ \hat{\boldsymbol{V}}(s) \end{bmatrix} = \begin{bmatrix} \hat{\boldsymbol{P}}_{\boldsymbol{S}}(\boldsymbol{s}) \\ \hat{\boldsymbol{W}}_{\boldsymbol{S}}(\boldsymbol{s}) \end{bmatrix} \tag{30}$$

IV. Circuit Formulation and Sensitivity Analysis

Consider a circuit $\mathcal{N}$ which contains linear lumped components, multiconductor transmission-line systems, and nonlinear elements. Without loss of generality, the time-domain MNA matrix equations for the circuit can be written as [24]

$$\boldsymbol{C}_{\mathcal{N}}\frac{d\boldsymbol{v}_{\mathcal{N}}(t)}{dt}+\boldsymbol{G}_{\mathcal{N}}\boldsymbol{v}_{\mathcal{N}}(t)+\sum_{k=1}^{K}\boldsymbol{P}_k\boldsymbol{i}_k(t)+\boldsymbol{i}_{NL}(\boldsymbol{v}_{\mathcal{N}}(t))=\boldsymbol{b}_{\mathcal{N}}(t) \tag{41}$$

where, $\boldsymbol{v}_{\mathcal{N}}(t)$ is a vector of size $N_{\mathcal{N}}$ containing the waveforms of the node voltages, independent voltage source currents, and inductor currents, $\boldsymbol{b}_{\mathcal{N}}(t)$ is a vector representing the excitations from the independent sources, $\boldsymbol{G}_{\mathcal{N}}$ and $\boldsymbol{C}_{\mathcal{N}}$ are constant matrices formed by linear lumped components, $\boldsymbol{i}_{NL}(\boldsymbol{v}_{\mathcal{N}})$ is a vector of functions describing the nonlinear components in the circuit, $\boldsymbol{P}_k$ is a $N_{\mathcal{N}}\times 2n_k$ selector matrix, with entries 1 or 0 that maps $\boldsymbol{i}_k(t)$ (the terminal currents of the kth line system) into the node space of the circuit $\mathcal{N}$, K is the number of MTL's, and n_k is the number of conductors in the kth MTL.

The transmission lines are described in the frequency domain by (32). For example, for the kth transmission-line system we have

$$(\boldsymbol{A}_k^R+s\boldsymbol{A}_k^I)\boldsymbol{V}_k(s)+(\boldsymbol{B}_k^R+s\boldsymbol{B}_k^I)\boldsymbol{J}_k(s)=\boldsymbol{F}_k(s),\quad k=1,\cdots,K \tag{42}$$

where

$$\boldsymbol{J}_k(s)=\begin{bmatrix}\boldsymbol{I}_k(s)\\ \hat{\boldsymbol{I}}_k(s)\\ \hat{\boldsymbol{V}}_k(s)\end{bmatrix} \tag{43}$$

and $\boldsymbol{F}_k$(s) is the vector of distributed sources for the kth MTL. In the time domain, the above equation becomes

$$\boldsymbol{A}_k^R\boldsymbol{v}_k(t)+\boldsymbol{A}_k^I\frac{d}{dt}\boldsymbol{v}_k(t)+\boldsymbol{B}_k^R\boldsymbol{j}_k(t)+\boldsymbol{B}_k^I\frac{d}{dt}\boldsymbol{j}_k(t)=\boldsymbol{f}_k(t),\quad k=1,\cdots,K. \tag{44}$$

Combined with (44), (41) is a first-order nonlinear differential equation and can be solved using the numerical-integration algorithms implemented in SPICE.

Let us now assume that the circuit $\mathcal{N}$ contains only linear elements. Combining the formulations for all transmission lines with the Laplace transform of (41), one obtains the frequency-domain MNA matrix for the circuit $\mathcal{N}$, shown in (45) at the bottom of the page, or, in the familiar compact form

$$(\overline{\boldsymbol{G}}+s\overline{\boldsymbol{C}})\boldsymbol{X}(s)=\overline{\boldsymbol{b}}(s). \tag{46}$$

From (30) to (32) and (46), it is immediately clear that the per-unit-length parameters of the MTL's appear explicitly in the MNA matrix of the overall circuit. Consequently, sensitivity analysis of the circuit responses with respect to any interconnect parameter can be performed in exactly the same manner as with respect to lumped-circuit elements [25]. More specifically, it is straightforward to show that the MNA matrix for sensitivity analysis of our circuit $\mathcal{N}$ is the same with the MNA matrix used for the simulation of the circuit. Indeed, suppose all responses $\boldsymbol{X}(s)$ have been obtained from the solution of (46). Let h be an interconnect parameter with respect to which response sensitivities are desired. Differentiation of (46) with respect to h yields

$$(\overline{\boldsymbol{G}}+s\overline{\boldsymbol{C}})\frac{\partial\boldsymbol{X}(s)}{\partial h}=\frac{\partial\overline{\boldsymbol{b}}(s)}{\partial h}-\left(\frac{\partial\overline{\boldsymbol{G}}}{\partial h}+s\frac{\partial\overline{\boldsymbol{C}}}{\partial h}\right)\boldsymbol{X}(s). \tag{47}$$

The calculation of the partial derivatives on the right-hand side (RHS) of (47) essentially involves calculation of the partial derivatives of the per-unit-length inductances, capacitances, resistances, and conductances of the MTL. Once these derivatives are known, sensitivity analysis of the circuit responses with respect to interconnect parameters can be performed in a straightforward fashion.

The time-domain sensitivity analysis is performed similarly. For simplicity, let us assume that the circuit contains only linear elements and we are using a fixed time-step trapezoidal integration. Then the solution at $t=n\Delta t$ is given as [25]:

$$\left(\overline{\boldsymbol{G}}+\frac{2}{\Delta t}\overline{\boldsymbol{C}}\right)\boldsymbol{x}(n\Delta t)=-\left(\overline{\boldsymbol{G}}-\frac{2}{\Delta t}\overline{\boldsymbol{C}}\right)\boldsymbol{x}((n-1)\Delta t)+\overline{\boldsymbol{b}}(n\Delta t)+\overline{\boldsymbol{b}}((n-1)\Delta t). \tag{48}$$

Differentiation of (48) with respect to h yields the desirable equation

$$\begin{aligned}\left(\overline{\boldsymbol{G}}+\frac{2}{\Delta t}\overline{\boldsymbol{C}}\right)\frac{\partial\boldsymbol{x}(n\Delta t)}{\partial h}&=-\left(\frac{\partial\overline{\boldsymbol{G}}}{\partial h}+\frac{2}{\Delta t}\frac{\partial\overline{\boldsymbol{C}}}{\partial h}\right)\boldsymbol{x}(n\Delta t)\\&\quad-\left(\frac{\partial\overline{\boldsymbol{G}}}{\partial h}-\frac{2}{\Delta t}\frac{\partial\overline{\boldsymbol{C}}}{\partial h}\right)\boldsymbol{x}((n-1)\Delta t)\\&\quad-\left(\overline{\boldsymbol{G}}-\frac{2}{\Delta t}\overline{\boldsymbol{C}}\right)\frac{\partial\boldsymbol{x}((n-1)\Delta t)}{\partial h}+\frac{\partial\overline{\boldsymbol{b}}(n\Delta t)}{\partial h}\\&\quad+\frac{\partial\overline{\boldsymbol{b}}((n-1)\Delta t)}{\partial h}.\end{aligned} \tag{49}$$

$$\begin{bmatrix}\boldsymbol{G}_{\mathcal{N}}+s\boldsymbol{C}_{\mathcal{N}} & [\boldsymbol{P}_1 00] & [\boldsymbol{P}_2 00] & \cdots & [\boldsymbol{P}_K 00]\\ (\boldsymbol{A}_1^R+s\boldsymbol{A}_1^I)\boldsymbol{P}_1^T & \boldsymbol{B}_1^R+s\boldsymbol{B}_1^I & \boldsymbol{0} & \cdots & \boldsymbol{0}\\ (\boldsymbol{A}_2^R+s\boldsymbol{A}_2^I)\boldsymbol{P}_2^T & \boldsymbol{0} & \boldsymbol{B}_2^R+s\boldsymbol{B}_2^I & \cdots & \boldsymbol{0}\\ \vdots & \vdots & \vdots & & \vdots\\ (\boldsymbol{A}_K^R+s\boldsymbol{A}_K^I)\boldsymbol{P}_K^T & \boldsymbol{0} & \boldsymbol{0} & \cdots & \boldsymbol{B}_K^R+s\boldsymbol{B}_K^I\end{bmatrix}\begin{bmatrix}\boldsymbol{V}_{\mathcal{N}}(s)\\ \boldsymbol{J}_1(s)\\ \boldsymbol{J}_2(s)\\ \vdots\\ \boldsymbol{J}_K(s)\end{bmatrix}=\begin{bmatrix}\boldsymbol{b}_{\mathcal{N}}(s)\\ \boldsymbol{F}_1(s)\\ \boldsymbol{F}_2(s)\\ \vdots\\ \boldsymbol{F}_K(s)\end{bmatrix} \tag{45}$$

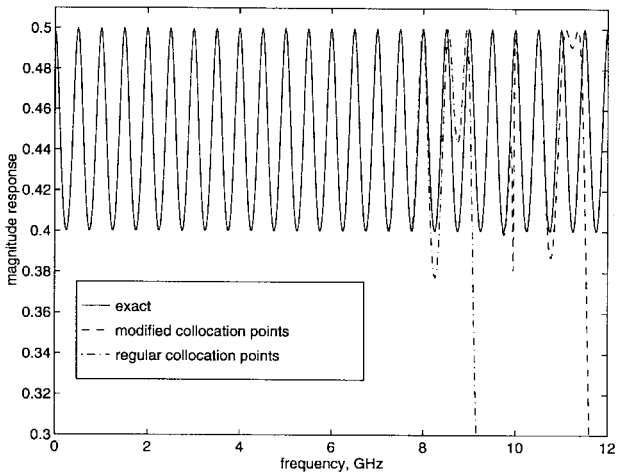

Fig. 1. The output frequency response of the circuit of Example 1.

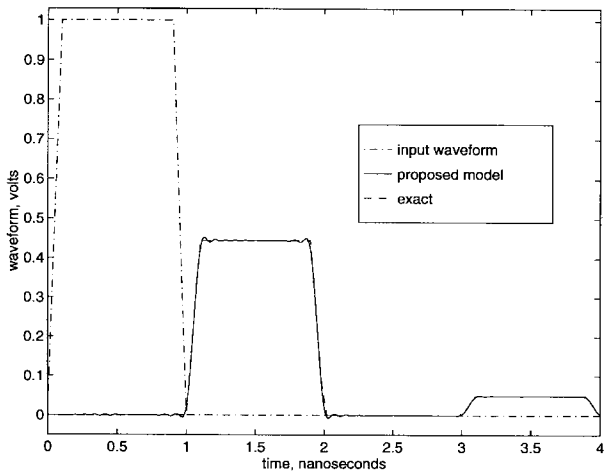

Fig. 2. The output transient response of the circuit of Example 1.

V. Numerical Experiments

In the following, a series of numerical examples are presented to demonstrate the validity of the proposed all-purpose transmission-line model and illustrate its application for signal distortion prediction in digital and analog circuits containing interconnects. SPICE3f4 [26] was used for the computer implementation of the proposed model. In all cases, the SPICE simulations did not exhibit any numerical instabilities. In general, numerical stability of spectral approximations of linear hyperbolic systems is of concern only when an explicit integration algorithm is used. For the stiffly stable integration algorithms used in SPICE, the proposed pseudospectral discrete models pose no numerical stability difficulties. For the sake of completeness, we mention that the numerical stability and convergence properties of spectral approximations of hyperbolic systems have been examined extensively in the literature [19], [27], and are well understood. As a brief summary we mention that if an explicit integration algorithm is used, the maximum allowable time step varies as $1/M^2$ for the standard Chebyshev pseudospectral approximation of order M. Clearly this leads to time steps much smaller than those used in conjunction with standard low-order finite-difference approximations, where typically the time step varies as $1/M$. However, as discussed in detail in [23], use of the shifted collocation points in the modified pseudospectral expansions of Section III helps relax the time-step constraint significantly.

Example 1: The first example deals with a simple lossless transmission line with per-unit-length parameters $L = 2.5$ nH/cm and $C = 1$ pF/cm. The line length is 20 cm. The phase velocity on the line is 20 cm/ns. The source and load impedances are resistive of value 25 Ω. We are interested in predicting the transient response of the line for a trapezoidal pulse of rise and fall times of 0.1 ns and width 1 ns. From (35), the maximum frequency of interest is predicted to be 10 GHz. Thus, the minimum wavelength is 2 cm, and (40) suggests that modified Chebyshev expansions of order at least 27 should be used for good accuracy. If instead, standard Chebyshev expansions were used, the order of expansions would be 42 according to (34).

Fig. 1 depicts the magnitude of the voltage response at the load resistor calculated using: 1) the exact result obtained from straightforward transmission-line theory; 2) the proposed model using a Chebyshev expansion of order $M = 30$; and 3) the proposed model using the modified ("stretched") Chebyshev method with collocation points given by (36) with $M = 30$ and $\alpha = 0.9$. It is clearly seen that use of the modified Chebyshev method leads to a highly accurate response up to 10 GHz in accordance with (40). On the other hand, use of the original Chebyshev method with $M = 30$ predicts the response accurately up to a frequency of about 7 GHz, in accordance with (40). The comparison of the transient response (predicted by the proposed model) with the exact response is shown in Fig. 2. Clearly, the proposed Chebyshev expansion-based model for the transmission lines accurately captures the wave properties of the solution (i.e., propagation delay and multiple reflections).

In order to demonstrate the superiority of the proposed Chebyshev expansion-based transmission-line model over the segmentation approach where the line is modeled as a cascade of several lumped circuits, this simple transmission-line circuit was also simulated using a 30-segment lumped-circuit approximation of the line. With the minimum wavelength of interest being 2 cm and a line length of 20 cm, this choice corresponds to a minimum wavelength resolution of three segments. The number of degrees of freedom used for the transmission-line modeling in the 20-segment approximation is the same with the one used for the Chebyshev model of order 30. The normalized errors in the frequency responses with respect to the exact solution are shown in Fig. 3. Clearly, Chebyshev expansions outperform the segmentation approach. Furthermore, this figure illustrates the benefit from using the modified ("stretched") Chebyshev method, namely, an increase in the bandwidth over which the error is kept below a specific level at the expense of a degradation in the exponential convergence of the approximation. To illustrate this point further, the normalized absolute error in the spatial distribution of the voltage is plotted in Fig. 4 for the case of $f = 8$ GHz. The modified Chebyshev expansion with the shifted collocation points provides for three orders

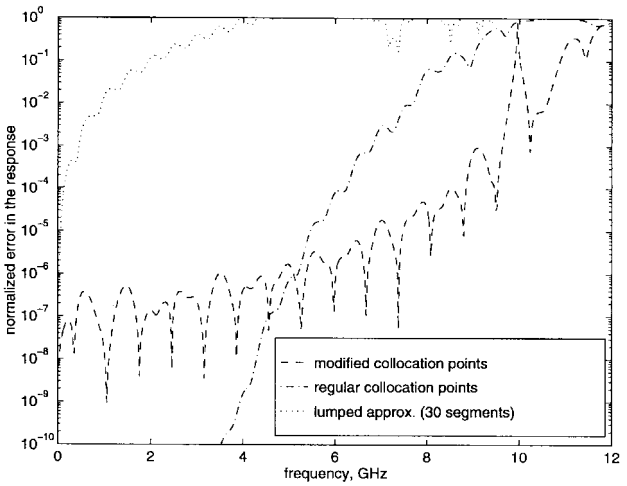

Fig. 3. Normalized error in the output frequency response of Example 1.

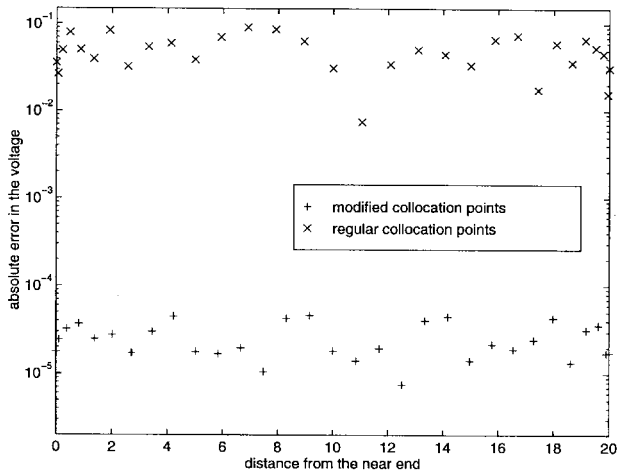

Fig. 4. The normalized error in the spatial voltage distribution for Example 1 at $f = 8$ GHz. The order of expansion is 30.

of magnitude better accuracy than the regular Chebyshev expansion.

Example 2: This example deals with the simulation of pulse propagation in the packaging interconnection system shown in Fig. 5. The two systems of coupled interconnects are identical, with length $l = 5$ cm and per-unit-length line parameters $L_{11} = L_{22} = L_{33} = 4.976$ nH/cm, $L_{12} = L_{23} = 0.765$ nH/cm, $L_{13} = 0.152$ nH/cm, $C_{11} = C_{22} = C_{33} = 1.082$ pF/cm, $C_{12} = C_{23} = -0.197$ pF/cm, $C_{13} = -0.006$ pF/cm, $R_{11} = R_{22} = R_{33} = 3.448$ Ω/cm. Dielectric losses are assumed negligible. The rise and fall times of the input voltage were taken to be 0.1 ns. The width of the pulse was 1 ns. With a minimum wavelength of interest of (approximately) 1.3 cm, the lines are about four wavelengths long at $f = 10$ GHz. Thus, Chebyshev expansions of order eight were used.

Fig. 6 compares the far-end voltage responses (calculated using the proposed model) for the active and victim lines with thoses obtained using the Berkeley SPICE lossy interconnect model. The purpose of this comparison was to validate the proposed model for the case of lossy lines. Excellent agreement is observed. It is pointed out that the lossy MTL model in Berkeley SPICE restricts coupling to adjacent lines only

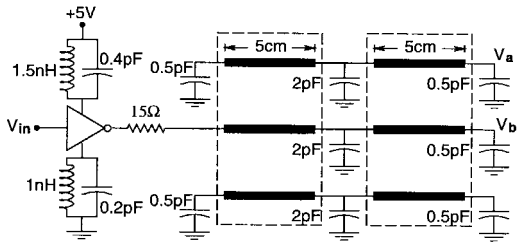

Fig. 5. The interconnect circuit for Example 2.

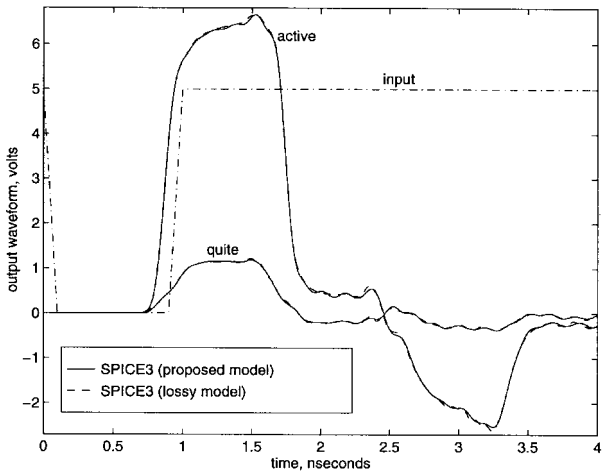

Fig. 6. Output transient waveforms for the interconnect circuit of Example 2.

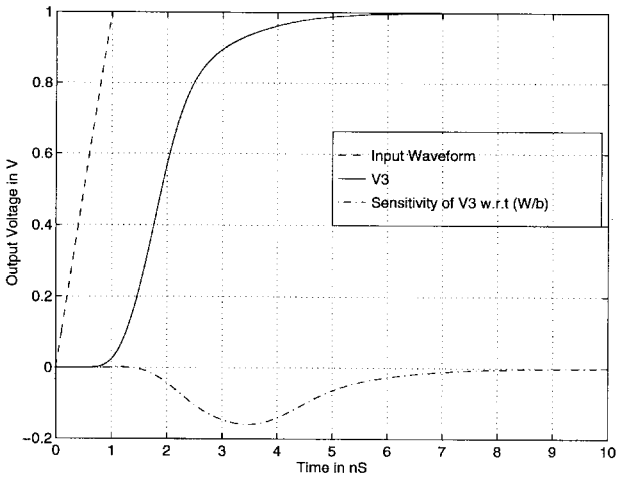

Fig. 7. Sensitivity of the capacitor voltage response with respect to stripline parameter $h = w/b$. The input pulse and the voltage response calculated for $w/b = 0.21$ and $\epsilon_r = 4$ are also shown for reference.

and requires all lines to be identical and equally spaced [7]. In contrast, the proposed model is completely general, even allowing for nonuniform MTL's and MTL's with frequency-dependent parameters, as discussed in detail in [13].

Example 3: The purpose of this example is to illustrate the application of the proposed MTL model for sensitivity analysis with respect to interconnect parameters. For this purpose, and without loss of generality, a balanced-stripline interconnect structure is considered. Let b be the ground-plane separation, w the width of the center-strip conductor, and ϵ_r the relative permittivity of the insulating medium. With the assumption

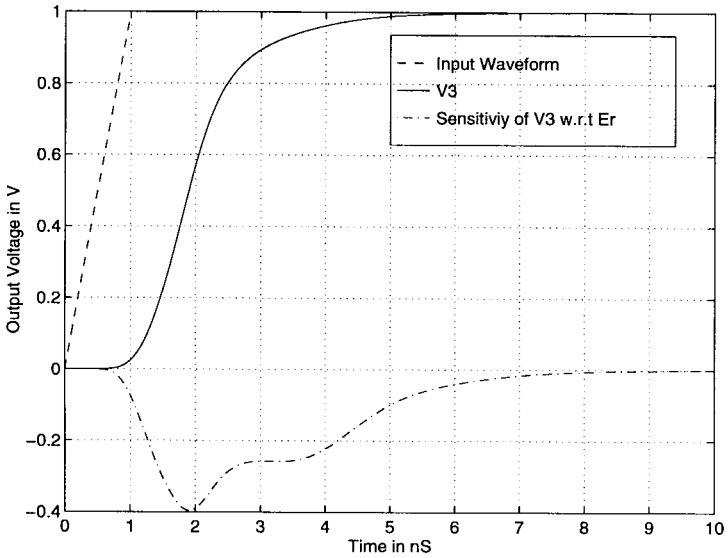

Fig. 8. Sensitivity of the capacitor voltage response with respect to stripline relative permittivity ϵ_r. The input pulse and the voltage response calculated for $\epsilon_r = 4$ and $w/b = 0.21$ are also shown for reference.

of perfect conductors and infinitesimally thin center strip, the characteristic impedance of the stripline is given in closed form by [28] as follows:

$$Z_0 = \frac{30\pi}{\sqrt{\epsilon_r}} \frac{K'(k)}{K(k)} \tag{50}$$

where $k = \tanh(\pi w/2b)$ and K represents a complete elliptic function of the first kind with K' its complementary function. An approximate expression for K/K' is

$$\frac{K'(k)}{K(k)} = \frac{1}{\pi} \ln\left(2\frac{1+\sqrt{k'}}{1-\sqrt{k'}}\right), \qquad 0 \le k \le 0.7 \tag{51}$$

with $k' = \sqrt{1-k^2}$. These expressions, combined with the pure TEM properties of the stripline, allow us to write closed-form expressions for the per-unit-length inductance L and capacitance C of the stripline

$$L = Z_0\sqrt{\epsilon_r}/c, \quad C = \sqrt{\epsilon_r}/(cZ_0) \tag{52}$$

where c is the speed of light in vacuum. Thus, the derivatives of L and C with respect to the interconnect parameters $h = w/d$ and ϵ_r can be obtained in a straightforward fashion.

A 15-cm section of stripline with $w = 31.5$ μm, $b = 150$ μm, and $\epsilon_r = 4$ was driven by a pulse generator and terminated at a 5-pF capacitor. The input impedance of the generator was taken to be resistive, with a value of 75.13 Ω. This is the value of the characteristic impedance of the stripline calculated from (50). To account for ohmic losses in the interconnect, the strip thickness t was taken to be 5 μm with conductivity $\sigma = 5.8 \times 10^7$ S/m. The per-unit-length resistance was obtained approximately using the simple expression $R = (\sigma w t)^{-1}$. The input pulse was a step of amplitude 1 V and rise time 1 ns. Figs. 7 and 8 depict the sensitivity of the voltage response at the capacitor with respect to the parameters h and ϵ_r, respectively. The voltage waveform at the capacitor is also depicted in both figures for the purpose of reference. The plotted sensitivities are actually the quantities $h(\partial V/\partial h)$ in Fig. 7, and $\epsilon_r(\partial V/\partial \epsilon_r)$ in Fig. 8.

The validity of the calculated sensitivities can be examined by considering the Taylor-series approximation for the time derivative of the voltage response

$$\frac{\partial V(h+\Delta h,t)}{\partial t} \approx \frac{\partial V(h,t)}{\partial t} + \Delta h \frac{\partial}{\partial t}\left(\frac{\partial V(h,t)}{\partial h}\right). \tag{53}$$

The characteristic time τ for the charging of the capacitive load C_L is proportional to the product Z_0C_L. As h increases, Z_0 decreases. Thus, τ is expected to decrease also. Faster charging of the capacitor implies an increase in the time derivative of the capacitor voltage response during the rise-time period of the incident voltage. From Fig. 7, $\partial^2 V(h,t)/\partial t \partial h$ is positive during this period, which yields, according to the equation above, an increase in $\partial V/\partial t$ for $h > 0$ as expected. At later times, the slope of V with time should be reduced, for the steady state to be reached faster as h is increased. This is confirmed by the negative value of $\partial^2 V(h,t)/\partial t \partial h$ during the later part of the transient response. Similar arguments apply for the sensitivity of the voltage response as ϵ_r is increased.

Example 4: This example is used to illustrate the impact that radiation noise can have on the IF output of the mixer in a receiver. The interconnect at the RF port of the receiver is taken to be a microstrip line of length 2 cm and per-unit-length parameters of $L = 3.7$ nH/cm and $C = 0.87$ pF/cm. The antenna is modeled by a time-harmonic voltage source with input resistance of 75 Ω. The frequency of the RF signal is 250 MHz and its magnitude is taken to be 20 mV. The LO signal has a magnitude of 10 mV and frequency 281.25 MHz. The mixer circuit used is shown in Fig. 9. The details of the values of the various components in this circuit can be found

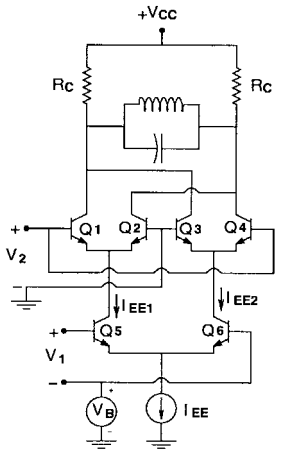

Fig. 9. The mixer circuit used in Example 4 (from [29]).

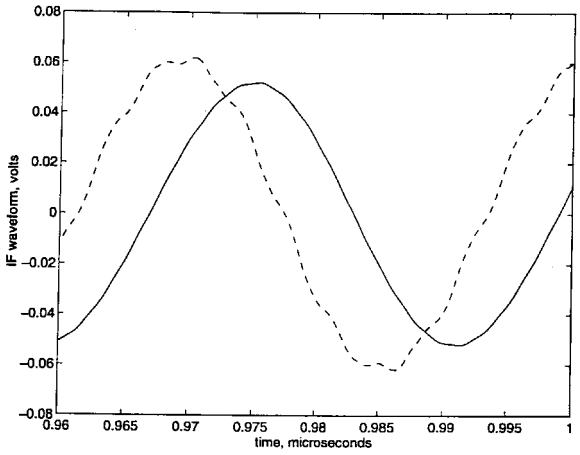

Fig. 10. Electromagnetic radiation coupled to the interconnect at the RF port of a mixer causes significant distortion of the IF output.

in [29]. The interfering noise is a periodic signal of Gaussian pulses. The period is taken to be 4 ns. Each Gaussian pulse in the periodic signal has an effective width of 4 ns also (i.e., each pulse is centered in the 4-ns interval which corresponds to one period). The 3-dB pulse width is taken to be $2\sqrt{0.7}$ ns. The model in [15] was used for the calculation of the distributed sources along the interconnects. The direction of propagation of the incident radiation is taken to be along the axis of the microstrip line, with the electric field linearly polarized in the direction perpendicular to the microstrip ground plane. The maximum amplitude of the electric field is 0.5 V/m. Fig. 10 compares the IF waveform in the absence of radiation noise (solid line) with that resulting when noise is present (dashed line). The resulting signal distortion is clearly illustrated.

VI. Conclusions

A new multiconductor transmission-line model has been presented for efficient and robust interconnect simulation using general-purpose nonlinear circuit simulators such as SPICE. The model is very general, in the sense that all types of interconnects, i.e., uniform, nonuniform, lossless, lossy/dispersive, can be handled. While the development of the model was given for the case of interconnects with frequency-independent per-unit-length parameters, the mathematical details for its extension to MTL's with frequency-dependent parameters is possible and has been presented in [13].

In addition to its modeling versatility, the proposed model has several other useful attributes which were discussed in detail in this paper. First, the use of (spectral) Chebyshev expansions for the spatial variations of the interconnect voltages and currents leads to numerical solutions of very high accuracy. In particular, this high accuracy is achieved using a very low spatial sampling of only three points per wavelength. Thus, interconnects which span several wavelengths at the highest frequencies of interest can be modeled very efficiently and accurately. Second, the proposed formulation is such that sensitivity analysis with respect to interconnect parameters can be effected in exactly the same manner used by standard-circuit simulators for sensitivity analysis with respect to lumped-element component values. This capability makes the proposed model very suitable for interconnect optimization.

Finally, coupling of electromagnetic radiation to interconnects can be modeled directly without the need for developing a new subcircuit. More specifically, the proposed model allows for the efficient simulation of such interactions in a SPICE-like simulator even when the victim lines are nonuniform. All that is needed is for the user to specify the values of the elements of the per-unit-length matrices at the collocation points used by the model. The same holds true for the incident field. Thus, fields with arbitrary spatial variation, subject (of course) to the constraints that make the transmission-line theory-based model for such interactions valid, can be accommodated.

A series of numerical experiments using a SPICE3f4 implementation of the model were presented in order to validate the model and demonstrate its attributes. In all validation studies, the calculated frequency and transient responses were found to be in excellent agreement with those obtained either from closed-form solutions or computer simulations using standard SPICE.

References

[1] A. J. Gruodis and C. S. Chang, "Coupled lossy transmission line characterization and simulation," *IBM J. Res. Develop.*, vol. 25, pp. 25–41, 1981.

[2] V. K. Tripathi and J. B. Rettig, "A SPICE model for multiple coupled microstrips and other transmission lines," *IEEE Trans. Microwave Theory Tech.*, vol. MTT-33, pp. 1513–1518, Dec. 1985.

[3] F. Y. Chang, "The generalized method of characteristics for waveform relaxation analysis of coupled transmission lines," *IEEE Trans. Microwave Theory Tech.*, vol. 37, pp. 2028–2038, Dec. 1989.

[4] J. E. Schutt-Aine and R. Mittra, "Nonlinear transient analysis of coupled transmission lines," *IEEE Trans. Circuits Syst.*, vol. 36, pp. 959–967, July 1989.

[5] J. Bracken, V. Raghavan, and R. Rohrer, "Interconnect simulation with asymptotic waveform evaluation," *IEEE Trans. Circuits Syst. I*, vol. 39, pp. 869–878, Nov. 1992.

[6] S. Lin and E. S. Kuh, "Transient simulation of lossy interconnects based on the recursive convolution formulation," *IEEE Trans. Circuits Syst. I*, vol. 39, pp. 879–892, Nov. 1992.

[7] J. S. Roychowdury, A. R. Newton, and D. O. Pederson, "Algorithms for the transient simulation of lossy interconnects," *IEEE Trans. Computer-Aided Design*, vol. 13, pp. 96–104, Jan. 1994.

[8] L. P. Vakanas, A. C. Cangellaris, and O. A. Palusinski, "Scattering parameter-based simulation of transients in lossy, nonlinearly terminated packaging interconnections," *IEEE Trans. Comp., Packag. Manufact. Technol., B*, vol. 17, pp. 472–479, Nov. 1994.

[9] E. Chiprout and M. S. Nakhla, "Analysis of interconnect networks using complex frequency hopping (CFH)," *IEEE Trans. Computer-Aided Design*, vol. 14, pp. 186–200, Feb. 1995.
[10] D. B. Kuznetsov and J. E. Schutt-Aine, "Optimal transient simulation of transmission lines," *IEEE Trans. Circuits Syst. I*, vol. 43, pp. 110–121, Feb. 1996.
[11] M. Celik and A. C. Cangellaris, "Efficient transient simulation of lossy packaging interconnects using moment-matching techniques," *IEEE Trans. Comp., Packag. Manuf. Technol. B*, vol. 19, pp. 64–73, Feb. 1996.
[12] R. Gupta, S.-Y. Kim, and L. T. Pillegi, "Domain characterization of transmission line models and analyzes," *IEEE Trans. Computer-Aided Design*, vol. 15, pp. 184–193, Feb. 1996.
[13] M. Celik and A. C. Cangellaris, "Simulation of dispersive multiconductor transmission lines by Padé approximation via the Lanczos process," *IEEE Trans. Microwave Theory Tech.*, vol. 44, pp. 2525–2535, Dec. 1996.
[14] C. R. Paul, *Analysis of Multiconductor Transmission Lines*. New York: Wiley, 1994.
[15] A. C. Cangellaris, "Distributed equivalent sources for the analysis of multiconductor transmission lines excited by an electromagnetic field," *IEEE Trans. Microwave Theory Tech.*, vol. 36, pp. 1445–1448, Oct. 1988.
[16] I. Wuyts and D. De Zutter, "Circuit model for plane-wave incidence on multiconductor transmission lines," *IEEE Trans. Electromag. Compat.*, vol. 36, pp. 206–212, Aug. 1994.
[17] A. Bayliss, C. I. Goldstein, and E. Turkel, "On accuracy conditions for the numerical computation of waves," NASA, Hampton, VA, Tech. Rep. 84-38, Aug. 1984.
[18] A. C. Cangellaris and R. Lee, "On the accuracy of numerical wave simulations based on finite methods," *J. Electromagnetic Waves Appl.*, vol. 6, pp. 1635–1653, 1992.
[19] C. Canuto, M. Y. Hussaini, A. Quarteroni, and T. A. Zang, *Spectral Methods in Fluid Dynamics* (Springer Computational Physics Series). Berlin, Germany: Springer-Verlag, 1987.
[20] O. A. Palusinski and A. Lee, "Analysis of transients in nonuniform and uniform multiconductor transmission lines," *IEEE Trans. Microwave Theory Tech.*, vol. 37, pp. 127–138, Jan. 1989.
[21] F.-Y. Chang, "Transient simulation of frequency-dependent nonuniform coupled lossy transmission lines," *IEEE Trans. Comp., Packag, Manufact. Technol. B*, vol. 17, pp. 3–14, Feb. 1994.
[22] M. Haque, A. El-Zein, and S. Chowdhury, "A new time-domain macromodel for transient simulation of uniform/nonuniform multiconductor transmission-line interconnections," in *Proc. 31st Design Automation Conf.*, San Diego, CA, June 1994, pp. 628–633.
[23] D. Kosloff and H. Tal-Ezer, "A modified Chebyshev pseudospectral method with an $O(N^{-1})$ time step restriction," *J. Comput. Phys.*, vol. 104, pp. 457–469, 1993.
[24] C. W. Ho, A. E. Ruehli, and P. A. Brennan, "The modified nodal approach to network analysis," *IEEE Trans. Circuit Theory*, vol. CAS-22, pp. 504–509, June 1975.
[25] J. Vlach and K. Singhal, *Computer Methods for Circuit Analysis and Design*, 2nd ed. New York: Van Nostrand, 1994.
[26] T. L. Quarles, "The SPICE3 implementation guide," Univ. California at Berkeley, Tech. Rep. Memo ERL-M98/44, 1989.
[27] A. Solomonoff and E. Turkel, "Global properties of pseudospectral methods," *J. Comput. Phys.*, vol. 81, pp. 239–276, 1989.
[28] I. Bahl and P. Bhartia, *Microwave Solid State Circuit Design*. New York: Wiley, 1988.
[29] D. Pederson and K. Mayaram, *Analog Integrated Circuits for Communications: Principles, Simulation & Design*. Norwell, MA: Kluwer, 1991, p. 436.

Mustafa Celik (S'89–M'90) was born in Konya, Turkey, in 1966. He received the B.S. degree in electrical engineering from the Middle East Technical University, Ankara, Turkey, in 1988, and the M.S. and Ph.D. degrees in electrical engineering from Bilkent University, Ankara, Turkey, in 1991 and 1994, respectively.

From 1994 to 1996, he worked in the Department of Electrical and Computer Engineering, University of Arizona at Tucson. He is currently a Research Associate in the Department of Electrical and Computer Engineering, Carnegie–Mellon University, Pittsburgh, PA. His research interests include circuit, interconnect, and mixed-signal simulation.

Andreas C. Cangellaris (M'86), received the Diploma in electrical engineering from the Aristotle University of Thessaloniki, Greece, in 1981, and the M.S. and Ph.D. degrees in electrical engineering from the University of California at Berkeley, in 1983 and 1985, respectively.

From 1985 to 1987, he was with the Electronics Department, General Motors Research Laboratories, Warren, MI. In 1987, he joined the Department of Electrical and Computer Engineering, University of Arizona at Tucson, first as an Assistant Professor (1987–1992) and then as an Associate Professor (1992–1997). In August 1997, he joined the Department of Electrical and Computer Engineering, University of Illinois at Urbana–Champaign, as a Professor. He has authored and co-authored over 100 scientific journal and conference papers in the areas of computational electromagnetics, microwave engineering, and modeling and simulation of high-speed interconnects. His expertise and research interests are in applied and computational electromagnetics, high-speed electronic packaging, and microwave engineering. Over the past ten years, he has supervised the development of electromagnetic software tools for the computer modeling of package parasitics and the simulation of pulse propagation in complex interconnect media in high-speed electronic packages.

Dr. Cangellaris is an associate member of the International Union of Radio Science (URSI). He received the URSI Young Scientist Award in 1993, and is an active member of the IEEE Antennas and Propagation, IEEE Microwave Theory and Techniques, and IEEE Components, Packaging and Manufacturing Technology societies. He is the co-founder of the IEEE Topical Meeting on Electrical Performance of Electronic Packaging, which is sponsored jointly by the IEEE Microwave Theory and Techniques Society and the IEEE Components, Packaging and Manufacturing Technology Society.

Abdul Yaghmour received the B.S. degree in electrical engineering from King Abdul-Aziz University, Jeddah, Saudi Arabia, in 1985, the M.S degree in electrical engineering from University of Arizona at Tucson, in 1996, and is currently working toward the Ph.D. degree.

From 1986 to 1991, he worked with Sony Electronics, Saudi Arabia, as a Design Engineer for audiovisual systems. He is currently a Research Assistant in the Electrical and Computer Engineering Department, University of Arizona at Tucson. His research interests include high-speed electronic packaging, semiconductor devices, and interconnects and mixed signal simulation.